Final Progress Report

DOE award #: DE-SC0010482

Award recipient Institution: Texas Engineering Experiment Station (TEES)

Project Title: **Deformation mechanisms of nanotwinned Al**

PI: Xinghang Zhang

Address: 3123 TAMU, Texas A&M University, College Station, TX 77843-3123

Telephone Number: (979) 845-2143

Email: zhangx@tamu.edu

DOE/Office of Science Program Office: Office of Basic Energy Science, Materials Science and Engineering Division

DOE/Office of Science Program Manager Contact: **Dr. John Vetrano**, 301-903-5976, john.vetrano@science.doe.gov

Date of the report and period covered by the report: **08/15/2013-08/14/2016**

Submission date: Nov. 10, 2016

I. A brief description of major accomplishments

The objective of this project is to investigate at a fundamental level, the deformation mechanisms of nanotwinned (nt) Al films with high density growth twins and stacking faults (SFs). Growth twins have been introduced into certain fcc metals with low stacking fault energy (such as Cu, Ag and 330 stainless steels) to achieve high strength, high ductility, superior thermal stability and good electrical conductivity. However, it remains a major challenge to produce growth twins and SFs in metals with ultra-high stacking fault energy, such as Al. Although deformation twins have been observed in nanocrystalline Al powders by low temperature, high strain rate cryomilling or in Al at the edge of crack tip or indentation (with the assistance of high stress intensity factor), these deformation techniques typically introduce twins sporadically and cannot control deformation twin density and thus affect the macroscopic material' properties.

During this 3-year project, we have performed in-depth studies on numerous subjects:
(1) investigate an intriguing twin formation mechanism in high stacking faulty energy metals;
(2) establish a novel technique to accurately determine strain rate sensitivity of nanotwinned and nanocrystalline metal films;
(3) summarize literature studies on growth twins in nt metals in a review article, Annual Review of Materials Research;
(4) inspect the occurrence of ITB migration and detwinning in nt metal at different stress and strain level;
(5) fabricate nt Al via template method and inspect the interaction of dislocations with TBs in nt Al, and
(6) study the mechanical stability of twin boundaries (TBs) and SFs in Al under stress, and work hardening of nt Al which were investigated by using in situ nanoindentation technique inside a transmission electron microscope. The followings are succinct summary of major findings from these studies.

The following sections briefly summarize some of the major accomplishment of this project.

I.1. Basic criteria for formation of growth twins in high stacking fault energy metals

(Kaiyuan Yu, postdoc, published in Applied Physics Letters, 2013)

It is well known that SFE plays an essential role on the formation of twins. Growth twins frequently appear in metals of low SFE, including Cu, Ag, and 330 SS, where they form spontaneously during deposition. In contrast growth twins are rarely observed in high stacking fault energy (SFE) metals, such as Al. After examining several multilayer systems, we derive the following criteria for introduction of growth twins into high SFE metals.

First, nucleation of twin seeds. It is important that a low SFE metals be used as a buffer or seed layer to nucleate high density growth twins. As mentioned previously nanotwins are frequently observed in metals with low SFE, thus having one of these metals as buffer in multilayer ensures the formation of twinned seeds. Second, coherency. A commonality among previous examples (Cu/Ni, Ag/Al and Cu/Fe(fcc)) all suggest that coherency is necessary so that twin seeds (in low SFE metals) can propagate through layer interface into high SFE components.

One question remains to be addressed: is it necessary to satisfy both criteria (nucleation of twins and coherency) to form nanotwins in high SFE metals? To answer this question, we constructed Ag/Ni multilayers with a focus on the formation of growth twins in Ni. The lattice mismatch between Ag and Ni is 14.9%, thus we suspect that nanotwins, which can be formed in

Ag, cannot penetrate into Ni due to a lack of coherent interface. As anticipated, XTEM micrographs of Ag/Ni 5 nm multilayer reveal incoherent layer interface (as shown by inserted SAD in Fig. 1a) and no sight of twins in Ni (Fig. 1b). Also highly {111} textured Ag/Ni 50 nm multilayer (in Fig. 1b) showed little evidence of growth twins in Ni. Layer interfaces in Ag/Ni 50 nm film have greater magnitude of waviness than that of Ag/Ni 5 nm film. Closer examination of certain location (Fig. 1c) of Ag/Ni 50 nm shows that TBs were occasionally observed in Ni adjacent to curved layer interface (Fig. 1d). This study thus strongly suggests that satisfaction of both criteria, twinned seeds and coherency, is probably necessary for formation of high density growth twins in high SFE metals.

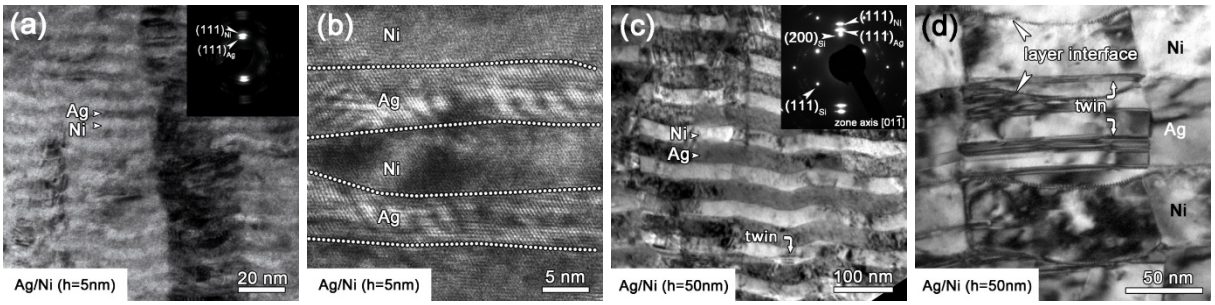

Figure 1. (a) XTEM micrograph of Ag/Ni 5 nm multilayers with strong {111} fiber texture examined from Si <110> zone axis, showing evident layer structure with an average columnar grain size of 50 nm. No twins were observed in Ni. (b) Corresponding HRTEM micrograph showing a lack of twins or stacking faults in Ag/Ni 5 nm multilayers. (c) XTEM image of Ag/Ni 50 nm multilayer observed from Si <110> zone axis showing sharp but wavy layer interface. The inserted SAD pattern shows strong {111} Ag and Ni texture aligned with Si (200) orientation. Twins were rarely observed in Ni. (d) XTEM image showing an incidence wherein growth twins were occasionally observed in Ni adjacent to curved layer interface.

The observation of growth twins in Ni adjacent to curved layer interface (Fig. 1d) does warrant further investigation. HRTEM micrograph in Fig. 2a reveals that TBs in Ag penetrated an inclined layer interface into Ni layer. By indexing fast Fourier Transformation (FFT) of several locations in Fig. 2b, we observed that at the curved interface, Ni (111) is connected (nearly parallel) to Ag (200) with a slight tilting angle of 9°, as labeled in Fig. 2d. Such inclined {111} planes then form a twin boundary in Ni, which can also be considered as an extension of the TB from Ag. Under this condition, Ag (200) planes are almost fully coherent with Ni (111) planes as shown in Fig. 2d, decorating with sporadic misfit dislocation. As displayed in Table 1, a lattice mismatch of only 0.64% exists between Ni (111) and Ag (200). In comparison, Fig. 2c shows a twin (lower one) that did not propagate from Ag into Ni layer where layer interface is relatively flat and incoherent. A much higher density of misfit dislocations appeared at the typical Ag/Ni layer interfaces where Ag and Ni {111} planes are parallel to each other (Fig. 2e). The mismatch strain in this case is 14.9%. The average separation distance of misfit dislocations, ~ 2 nm in Fig. 2e, is consistent with such a large lattice mismatch.

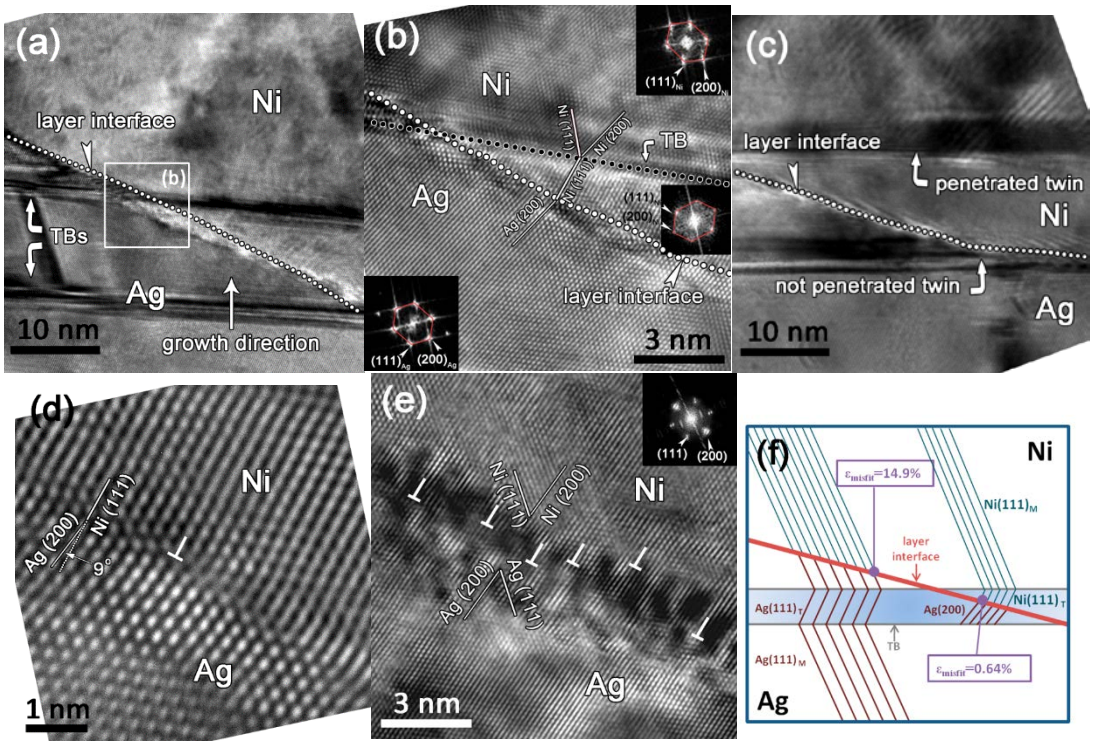

Figure 2. A new mechanism enabling the formation of growth twins in Ni with assistance of curved layer interface. (a) HRTEM image showing twin boundaries in Ag penetrate through layer interface into Ni. (b) Magnified area as indicated by a box in (a). Plane indices were revealed from the inset fast Fourier transformation (FFT). The formation of twin boundary in Ni is assisted by coherency between Ag (200) and Ni (111) planes across the curved layer interface. The epitaxially grown Ni (111) crystal (on Ag (200)) became a twinned variant with the Ni matrix. (c) HRTEM showing the lower twin did not penetrate the Ag/Ni layer interface due to the lack of local coherency. (d) HRTEM micrograph at higher magnification reveals the orientation relationship between coherent Ag (200) and Ni (111). Misfit dislocations were rarely observed. (e) HRTEM micrograph reveals the regular semicoherent Ag (111)/Ni (111) interface decorated with an array of high-density misfit dislocations. (f) Schematic of twin formation mechanism illustrating the significance of coherency (between Ag (200) and Ni (111) across curved layer interface) on formation of growth twins in Ni. In contrast misfit dislocations will be generated across regular Ag and Ni (111) interface.

In general, nanotwins in Ag are rarely able to penetrate the incoherent (or semicoherent) Ag (111) /Ni (111) layer interfaces. This observation again validates that the introduction of twins in high SFE metals may require simultaneous satisfaction of both criteria (coherency and twin seeds). The observation of twin penetration event across Ag/Ni interface, appearing as an exception at the first glance, is in fact in agreement with these criteria. In this particular case TBs in Ag penetrate a coherent dissimilar interface between Ag (200) and Ni (111). Here “dissimilar” refers to the dissimilar planar indices of two phases. A schematic of this twinning mechanism is shown in Fig. 2f. The Ag/Ni interface exhibits two different orientation relationship, which are Ni (111)//Ag (111) and Ni (111)//Ag (200) depending on the location adjacent to the curved layer interface. Arrays of misfit dislocations develop across incoherent Ag (111)/Ni (111) interface, whereas TBs (nucleated in Ag) penetrate coherent Ag (200)/Ni (111) interface and expand into Ni.

Note that the presence of a curved layer interface makes the formation of coherent interface possible.

We derive two important criteria that enable the propagation of growth twins across layer interfaces into high SFE metals. These are summarized as (i) a low SFE buffer layer that readily forms twin seeds, and (ii) global coherency between coherent similar interfaces (between constituents with identical planar indices) or local coherency between coherent dissimilar interfaces (between constituents of different planar indices) that permits twins to propagate across layer interfaces. The formation of twin boundaries across layer interface could be a natural consequence of strain relaxation, in competition to the formation of misfit dislocations.

I.2. A new method for reliable determination of strain-rate sensitivity of low-dimensional metallic materials by using nanoindentation (Y. Liu, graduate student, Scripta Mater., 2014)

Nanoindentation is increasingly used to determine the strain rate sensitivity (SRS) of materials with small volumes, such as nanocrystalline metal films. However traditional data analysis yields large scattering and uncertainty due to the influence of thermal drift on displacements measured at low strain rates. Here we use a new method that renders hardness insensitive to thermal drift. The method involves (a) directly measuring contact stiffness by means of a small dynamic oscillation and (b) calculating contact area from the measured contact stiffness and the elastic modulus, which is insensitive to strain rate. The new technique is validated on nanocrystalline Ni and nanotwinned Cu films and returns expected values of SRS.

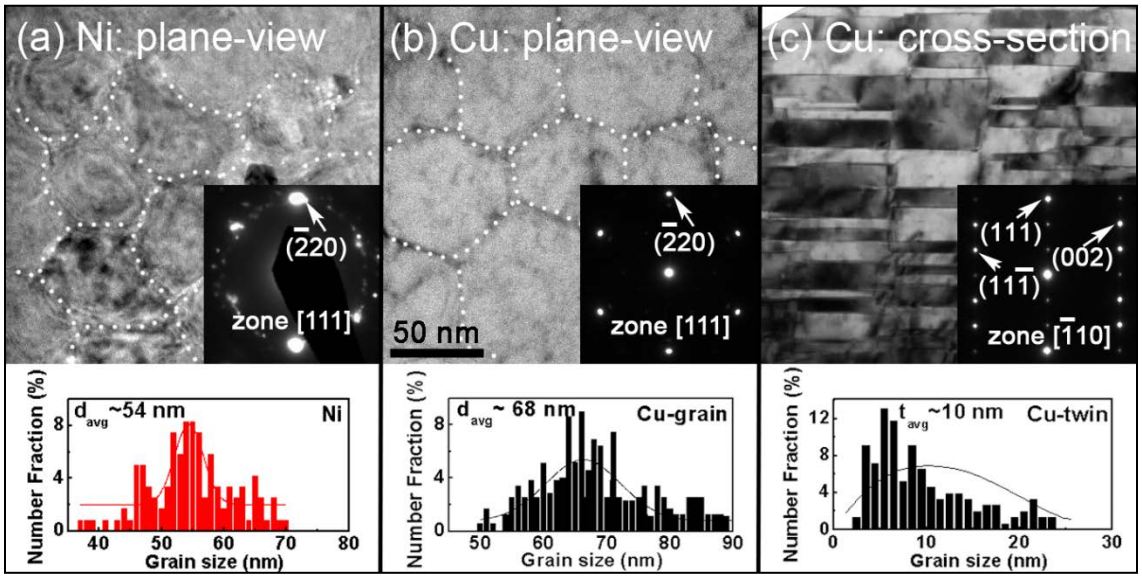

Figure 3. Plane-view TEM micrographs of (a) sputter-deposited nanocrystalline (nc) Ni (111) and (b) epitaxial nanotwinned (nt) Cu (111) films. Statistical analysis shows that the average grain size d_{ave} for nc Ni is ~55 nm, and the d_{ave} for nt Cu is also ~55 nm. (c) Cross-section TEM micrograph of the epitaxial nt Cu display high density growth twins with an average twin spacing of ~ 10 nm as evidenced by the corresponding statistical study.

To validate the modified method, we selected two systems, sputtered nt Cu and nc Ni films. The plan-view TEM micrograph of the nc Ni in Fig. 3a shows numerous grains and the statistical grain size distribution analysis yields an average grain size of ~54 nm. The inserted selected diffraction (SAD) pattern displays a strong (111) texture of the film. The plan-view TEM micrograph of the nt Cu film and corresponding SAD pattern in Fig. 3b present an epitaxial (111) single-crystal-like film with an average grain size (shown from the underneath grain size distribution chart) of ~ 68 nm. A cross-section TEM micrograph (Fig. 3c) of the same Cu specimen (examined along Cu <110> zone axis) shows the epitaxial (111) Cu film contains an extremely high density of nanotwins with an average twin spacing of 10 nm.

Next we compare the results obtained by the two methods from the same sets of indentation data. As shown in Fig. 4a, the conventional technique has substantial scattering at lower strain rate, whereas the modified method leads to tight convergence of different sets of data at all strain rates. The calculated indentation hardness vs. indentation displacement in Fig. 4b exhibits the following characteristics. First the indentation hardnesses calculated from both techniques are similar at a high strain rate (0.05/s), 7.5 GPa. Second, at the intermediate strain rate (0.01/s), the conventional analysis (black traces) leads to prominent scattering in hardness, 7.9 ± 1 GPa, in comparison to 7.4 ± 0.1 GPa obtained from the modified method (red traces). Third, when a lower strain rate 0.002/s was applied, significant scattering results in unacceptable hardness, 22 ± 7 GPa obtained from the conventional method. Conversely, the hardness results derived from the modified method has substantially improved convergence and reliability, 7.2 ± 0.1 GPa. Finally, the values of E determined by conventional method at low strain rate (0.002/s) is unreliable, ~ 500 GPa, comparing to the bulk (literature) value of 220 GPa for Ni. Fig. 5a-b compares the SRS values calculated from strain-rate-dependent hardness values obtained by the two methods for nt Cu and nc Ni films. The conventional analysis (open squares) yields erroneous results, as indicated by negative large SRS values for both specimens. However, the modified method (solid circles) yields a reasonable positive SRS value for nc Ni: m = 0.016 ± 0.002, and for nt Cu: m = 0.020±0.002.

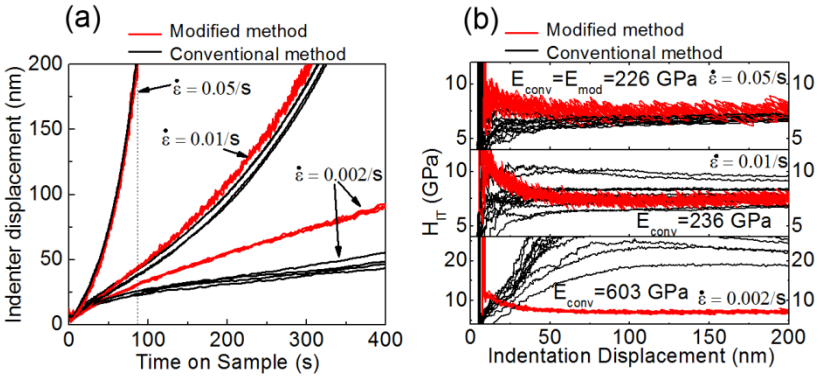

Figure 4. Comparing conventional (black) and new (red) methods using the same data on nc Ni. (a) Displacement vs. indentation time obtained at various strain rates. (b) Calculated indentation hardness vs. displacement plots. The conventional technique has substantial scattering at lower strain rate, whereas the new method leads to tight convergence of different sets of data.

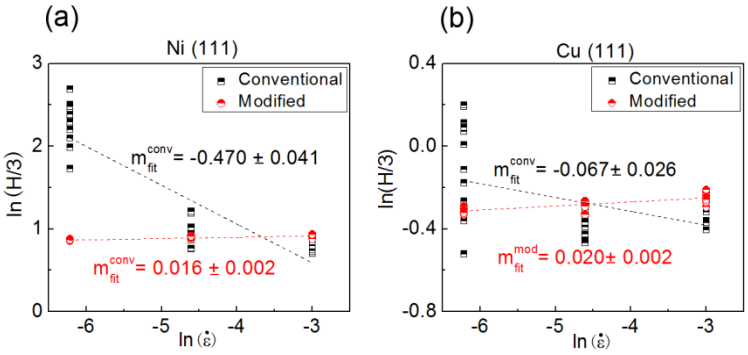

Figure 5. Comparison of SRS calculated from two methods for nt Cu and nc Ni films. The conventional analysis (half filled squares) yields erroneous results, as indicated by a negative SRS values. In contrast, the new method (show by solid circles) produces a reliable positive SRS value for nc Ni and nt Cu.

I.3. Review on growth twins in nanostructured metals (Ann. Rev. Mater. Research, 2014)

This article reviews recent basic research on two classes of twins: growth twins and deformation twins. We (Beyerlein, Zhang, Misra) focus primarily on studies that aim to understand, via experiments, modeling, or both, the causes and effects of twinning at a fundamental level. We anticipate that, by providing a broad perspective on the latest advances in twinning, this review will help set the stage for designing new metallic materials with unprecedented combinations of mechanical and physical properties. In this paper, we summarized the synthesis of growth twins in nt Al, and thermal stability of twin boundaries in nt metals. Additionally, we have identified the following challenges and future Prospects in nanotwinned metal research.

The progress made in NT metals has inspired new directions and challenges for future research in this area. First, there is a need to synthesize bulk NT materials. Recent studies have demonstrated that nanotwins can be introduced into bulk steels and superalloys.The radiation response of NT metals is also largely unexplored. Severe radiation damage poses significant challenges to the application of metallic materials in nuclear reactors. The interaction of nanotwins with radiation-induced point defects was recently investigated. Although CTBs appear to have a low sink efficiency for point defects and He, ITBs seem to be effective defect sinks. Furthermore, the migration of both CTBs and ITBs under irradiation conditions can remove defect clusters such as SF tetrahedra. Because detwinning is frequently observed in NT metals, it is worthwhile to develop microstructural design strategies to induce solute segregation or precipitation at TBs to stabilize nanotwins under high stresses and temperatures.

I.4. Plasticity and ultra-low stress induced twin boundary migration in nanotwinned Cu by *in situ* nanoindentation studies (Y. Liu, postdoc, published in Applied Physics Letters, 2014)

Engineering grain size has been a major strategy to strengthen metals, given that high angle grain boundaries resist the dislocation transmissions. However, the enhanced mechanical strength is at expense of compromising ductility. In comparison, high strength nt metals equip themselves with (111) CTBs which set up obstacles to dislocation slip transfer events. Meanwhile, nt metals exhibit better ductility, thermal stability, electrical conductivity, creep and fatigue resistance.

The plasticity and twin migration events have been intensively studied. Previous studies have suggested that detwinning happens in plastically deformed nt metals and molecular dynamics simulations predicted that fine twins can migrate at low stress, but little *in-situ* evidence has validated those predictions. Hence, we have several important questions

that remain unanswered experimentally: (1) what is the magnitude of stress necessary for ITB migration? (2) how do dislocations nucleate in nt metals during deformation? (3) does ITB migration occur simultaneously with nucleation of dislocations? (4) does ITB migration account for plastic yielding? Therefore, the technique, namely *in-situ* observations of twin migration activities and plasticity in nt metals under the transmission electron microscope, is necessitated to address these questions.

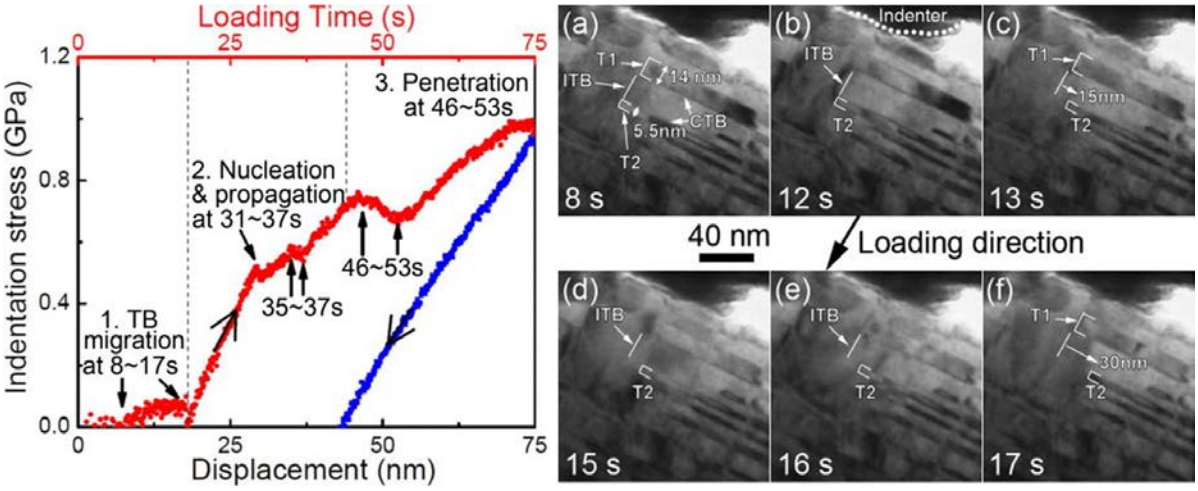

Figure 6. *In-situ* nanoindentation study that shows the elastic and plastic deformation of epitaxial nt Cu indented along <111> direction. Indentation stress *vs.* displacement plots during loading (red, color online) and unloading (blue, color online) process. And sequential *in-situ* TEM snapshots revealing the migration of ITB during 8–17 s, corresponding to stress plateau in the ultra-low stress regime as indicated in indentation stress *vs.* displacement plot. (a) Two nanotwins, T1 and T2, were identified with thickness 14 and 5.5 nm, respectively. A short straight line near the initial ITB location was highlighted as a reference. The ITBs are stable during loading up to 12 s (b). (c) By 13 s, during deformation, the thinner twin T2 migrated rightward by 15 nm. Continuous deformation rebuilds the stress field around the ITB at 15 s (d). Up to 16~17 s ((e)–(f)), and another prominent ITB migration event by 15 nm was captured. The ITB has migrated a total of 30 nm over this period.

A typical indentation stress *vs.* displacement (and time) plot captured during loading and unloading processes for epitaxial nt Cu. Basically, the loading segment can be grouped into three regimes corresponding to three drastically different microstructural evolution events. First, in zone 1, a clear stress plateau was observed between 8 and 17 s when the thinner twin (T2) with 5.5 nm spacing migrated about 30 nm away from the starting point and the migration occurred at ~ 0.1 GPa, much lower than the stress for macroscopic yielding. Our *in-situ* study clearly shows that some of the fine nanotwins started detwinning before the nucleation of dislocations, but it was unclear prior to our study.

Second, a linear stress-displacement plot was recorded in zone 2. The stress rose linearly until 0.5 GPa (at 31 s), at which non-linear deviation is prominent thereafter. As shown in Fig. 7(b) (30 s), dislocation started their nucleation under the indenter tip. At 31 s (Fig. 7c), an avalanche of dislocation loops occurred corresponding to the onset of non-linear deviation of stress. The avalanche of dislocation loops during nucleation event led to an increase of dislocation density from nearly negligible to ~ 5×10^{11} cm^{-2} in less than a second.

We captured the microscopic yielding event due to nucleation of dislocations at lower stress (~ 0.5 GPa). Two factors caused the succeeding prominent work-hardening (31–35 s). First, the rapid increase in dislocation density under indenter may require greater stress to continuously nucleate dislocations. Second, the interactions between mobile dislocations and these high density dislocation loops may also lead to work hardening. The rapid propagation of dislocations towards the CTB (T3) might have led to an insignificant kink (a small load drop) at 35 s. At 37 s, it is evident that dislocations approached the CTB. As dislocations encounter resistance from the CTB, it is necessary to increase external stress to continuously pile up dislocations at the CTB, that is, work hardening occurs (37–46 s).

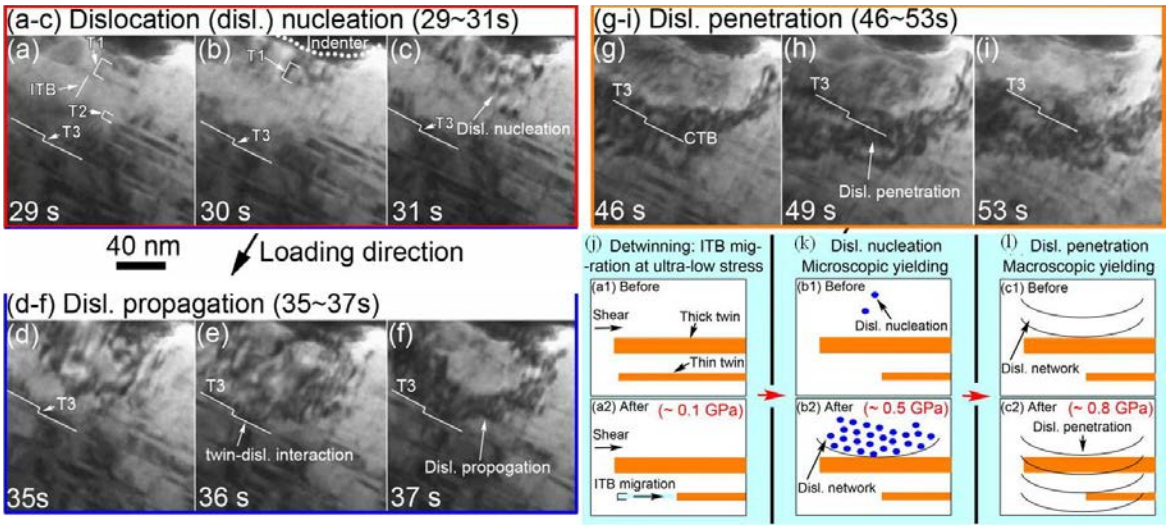

Figure 7. Sequential *in-situ* TEM snapshots reveal the dislocation nucleation, propagation, and penetration events in plastic regime. (a)–(c) Nucleation of dislocation. (a) Geometry and location of T1, T2, and T3 (a CTB). As shown in (b), dislocations started to nucleate at 30 s, and the formation of multiple dislocations was captured at 31 s (c). (d)–(f) Propagation of dislocations towards TBs. During 35–37 s, the group of dislocations propagated rapidly towards T3. The migration of dislocations was hindered by T3. Simultaneously, a large dislocation loop consisting of a band of dislocations was blocked by T3. (g)–(i) Dislocation penetration across TBs. During 46–53 s, the band of dislocations penetrated through TBs. Schematics were drawn to demonstrate the stress induced evolution of microstructures during *in-situ* nanoindentation of nt Cu.

Zone 3 is characterized by a prominent load drop at 46 s at a stress level of ~ 0.8 GPa. The load drop appeared to reach its minimum at 53 s, before the load increased again nonlinearly. In zone 3, the interaction between dislocations and T3 was captured. As shown in Fig. 7g&h, the dislocation band started to penetrate T3, and the dark band appeared completely transmitted across T3 by 53 s (Fig. 7i). During the penetration event, prominent load drop was observed. The piled-up dislocations eventually penetrated the CTB (46–53 s) accompanied by substantial load drop. We notice that the stress at which penetration events occur (~ 0.8 GPa) compares well to macroscopic yielding. The general perception of macroscopic yielding in nt metals has been attributed to dislocation penetration through TBs, validated by our *in-situ* nanoindentation studies.

We identified ultra-low indentation stress induced ITB migration at ~ 0.1 GPa, an event that is clearly non-elastic and irreversible. Dislocation nucleation at ~ 0.5 GPa leads to non-linear stress deviation from elastic regime, signaling a microscopic yielding event,

followed by work hardening presumably dominated by dislocation nucleation. Finally, at the stress corresponding to macroscopic yielding (~ 0.8 GPa), dislocations were able to transmit across CTBs. This study provides an important forward step to understand the deformation physics of nt metals, in particular, the correlation among several non-elastic deformation processes, including ITB migration, dislocation nucleation, and transmission across CTBs.

I.5. *In situ* nanoindentation studies on deformation mechanisms of nanotwinned Al

(Daniel Buffor and Yue Liu, graduate students, Nature Communications, 2014)

Nanotwinned (nt) metals stirred significant interest lately because Σ3{111} coherent twin boundaries (CTBs) contribute to high strength and ductility, enhanced electrical conductivity, and superior thermal stability. Most prior studies have focused on nt metals with low stacking fault energy (SFE), such as Ag, Cu and stainless steels. In contrast, the plasticity of high SFE nt Al has not been investigated because the difficulty in fabricating high density growth twins in Al. Here we report exceptional work hardening and plasticity in nt Al containing abundant Σ3{112} incoherent twin boundaries (ITBs) based on *in situ* nanoindentation studies inside a transmission electron microscope (TEM) and corresponding molecular dynamics (MD) simulations. MD simulations also reveal drastic differences in plastic deformation between nt Cu and nt Al ascribed to the SFE-controlled dislocation-ITB interactions. This study provides new insight into ITB dominated deformation mechanisms in high SFE nt metals, and provides a starting point to explore plasticity for a new spectrum of high SFE nt metallic materials.

In this study, epitaxial {111} nt Al films were fabricated and contained abundant ITBs and occasional CTBs (Fig. 8a). The cross-section TEM micrograph in Fig. 8c shows a straight ITB separating two domains, and the inset selected area diffraction (SAD) patterns reveal the twinned orientation between these domains. A high-resolution TEM micrograph (Fig. 8c-d) reveals the atomic arrangement of a straight ITB. The average domain size was ~200 nm.

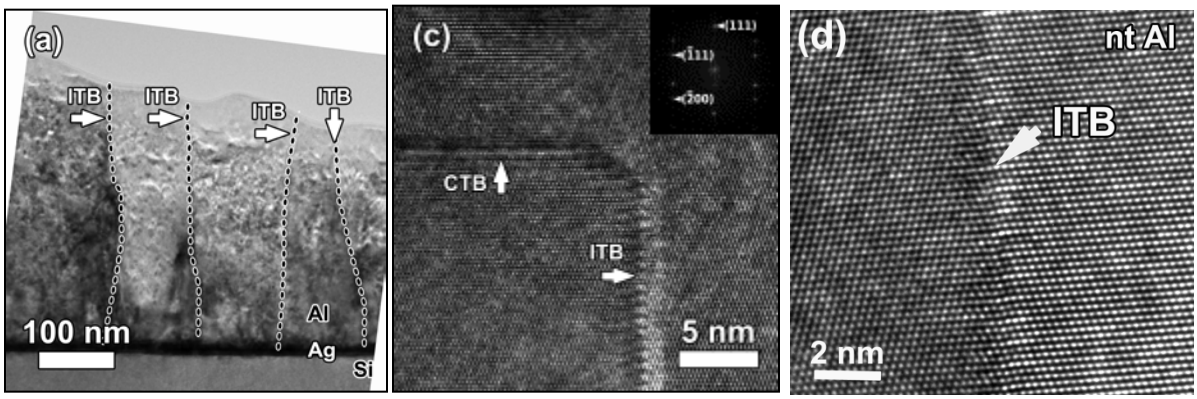

Figure 8. Overview of nanotwinned (nt) Al with abundant incoherent twin boundaries (ITBs) and certain coherent twin boundaries (CTBs). (a) Cross-section TEM micrograph (Al $<01\bar{1}>$ zone axis) showing an overview of the typical nt Al film structure with predominately ITBs; the Si substrate, epitaxial Ag seed layer, and epitaxial nt Al domains are visible. A typical higher magnification TEM micrograph shows that two ITBs extending vertically through the film. The inset selected area diffraction pattern confirms the epitaxy and ITB structure of the nt Al film. (c) HRTEM micrograph showing an example of an ITB/CTB

junction in nt Al film. The structure of each type of twin boundary is readily apparent. The inset fast Fourier transform (FFT) of the micrograph confirms the formation of twin boundaries. (d) An HRTEM micrograph that shows atomic arrangement surrounding an ITB in nt Al film.

Via in situ nanoindentation, multiple indentation cycles were performed at the same location to investigate deformation mechanisms. We have observed dislocation nucleation, dislocation absorption by the ITB, dislocation pile-up on the ITB and dislocation transmission across the ITB. These findings will be briefly summarized as follows.

I.5.1. Serrated stress drops during dislocation nucleation and strain burst

During *in situ* nanoindentation of nt Al, we observed serrated stress drops (strain bursts), the magnitude of which substantially exceeded the noise level. Strain bursts have been frequently observed during micropillar compression tests of various metallic materials and have long been considered a consequence of dislocation nucleation events. During indentation of nt Al, each strain burst was typically correlated to the nucleation of dislocations. The stress-drop associated with most strain burst events was generally low, ~ 10 MPa, as only individual dislocations were nucleated. However, during dislocation avalanches, sizable semicircular dislocation loops nucleated (e.g. Fig. 9d-e), accompanied by substantial stress-drops (Fig. 9a), approaching 50 MPa in some cases. Interestingly MD simulations also predicted serrated stress-strain curve in nt Al, drastically different from low SFE nt Cu or Ag. Discrete dislocation dynamics (DDD) simulations predicted that dislocation avalanches are a universal phenomenon during deformation of single crystal Al and grain boundaries in polycrystalline Al would reduce avalanche frequency. Micropillar compression tests on Al yield controversial results presumably related to the orientation of grain boundaries.

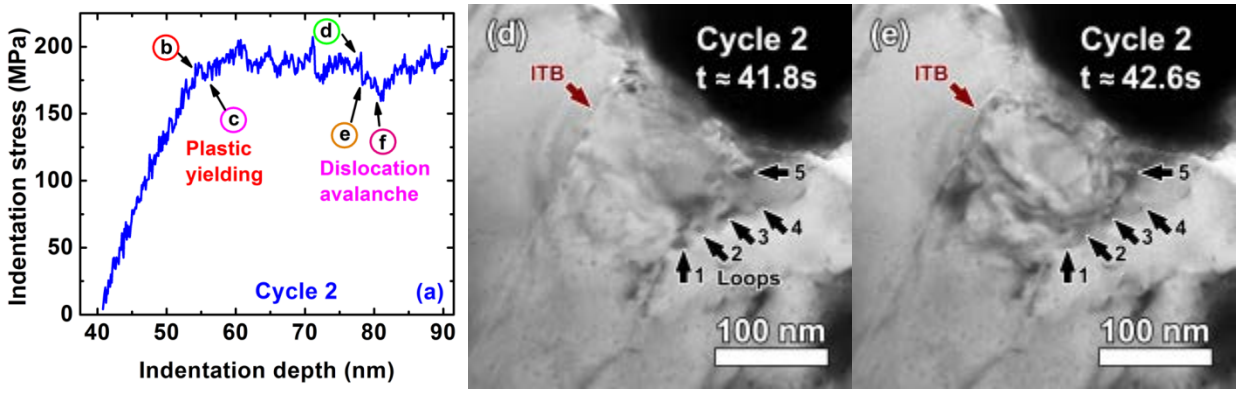

Figure 9. Sequential snap shots taken during indentation cycle 2 revealing nucleation and avalanche of dislocations during plastic deformation of nt Al confined by the ITB. (d) t ≈ 41.8 s: just before a distinct stress drop, Dislocations were active beneath the indenter, and several sessile loops had been generated (labeled by black arrows). (e) t ≈ 42.6 s: in less than one frame, an oval-shaped avalanche of large dislocations (~ 130 nm in diameter) appeared, accompanied by a substantial load drop. Loops were pinned by sessile dislocation loops (arrows 1-5) on the right, and blocked by the ITB on the left.

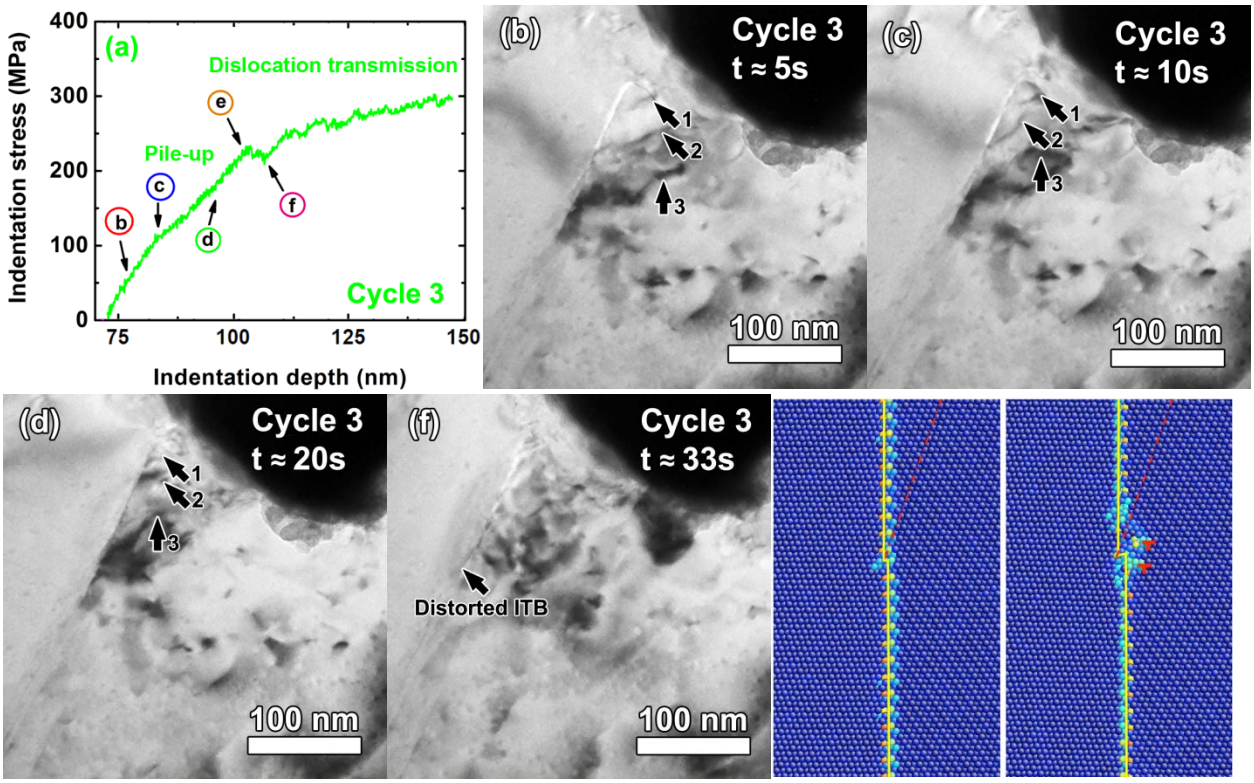

Figure 10. Sequential snap shots taken during indentation cycle 3 revealing apparent dislocation pile up before transmission event across the distorted ITB. (a) Corresponding stress-displacement curve with arrows indicating the following TEM micrographs. (b) t ≈ 5 s: the morphology of dislocations before moving towards to the ITB. (c) t ≈ 5 s at ~150 MPa, dislocations start to pile up against the ITB. (d) t ≈ 20 s: dislocations networks start forming while more dislocations are combined. (f) t ≈ 33 s: formation of distorted ITB (step or kink) after interaction with incoming dislocations. (g-h) atomic structures showing a lattice dislocation entering am initial ITB (left), and two lattice dislocations entering the ITB (right). The blocking mechanism is the lattice dislocation dissociates into an interface disconnection. The residual component is sessile and corresponds to the formation of step or kink.

I.5.2. The ITB-dislocation interactions in nt Al

During *in situ* nanoindentation of nt Al, we observed lattice dislocation piling up on ITBs and the formation of distorted ITB, before dislocations transmitting through the ITB as shown in Fig. 10. We applied a MD simulation to further understand this phenomenon. We used a twinned bicrystal model for Al to examine interface disconnection formation by single dislocations in detail. Three 60° mixed dislocations move towards an ITB under shear stress of 200 MPa at 10 K. Nucleation of the interface disconnection results from dissociation of the 60° mixed dislocation at the ITB, which is described as $\frac{1}{2}[101]=\frac{1}{3}[111]+\frac{1}{6}[1\bar{2}1]$. The residual $\frac{1}{6}[1\bar{2}1]$ component remains on the ITB $(11\bar{2})$ plane, and appears as a step (Figs. 10f). Thus, lattice dislocations were not able to penetrate ITBs due to the inherently high resistance of ITBs to the dislocation dissociation. These MD simulations thus lend more support to work hardening in nt Al via ITBs.

I.6. The mechanical stability of ITBs in nt Al

In nt Al, the ITB migration accommodated plasticity at greater stress can be explained by the interface disconnection glide (IDG) mechanism revealed by MD simulations. First, lattice dislocations dissociate at the ITB, causing its migration accompanied by load drop. Next, an interface disconnection dipole or loop nucleated at the ITB under high shear stress (parallel to the ITB), and the growth of interface disconnections can lead to ITB migration. Short steps or kinks consisting of ITB/CTB junctions are less stable energetically than straight ITBs, and are likely sites for easier migration. The ITB segment in nt Al showed an instantaneous migration velocity of ~ 8 nm/s from our *in situ* studies. The high stress (500 MPa) at which ITB migrates implies that nt Al should have high strength and yet with ITB accommodated plasticity.

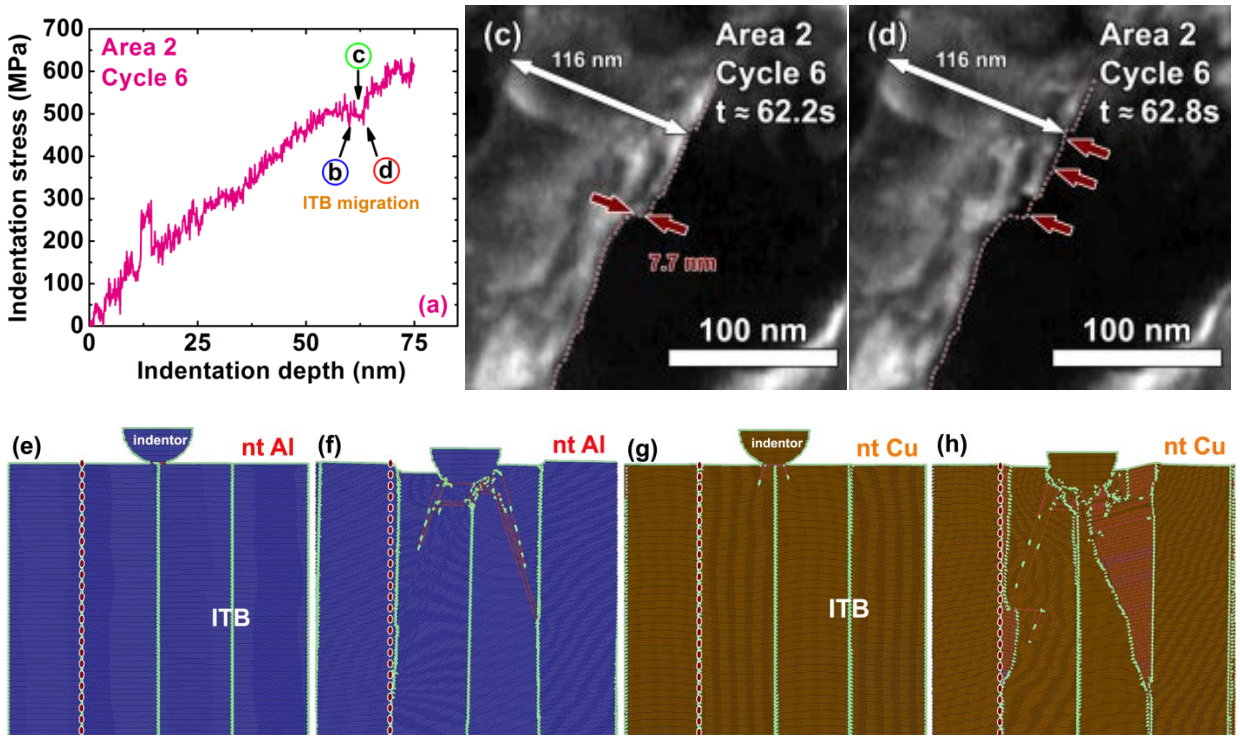

Figure 11. (a-d) Sequential snap shots revealing substantial ITB migration. (a) Stress-displacement curve after 6 prior indentation cycles, with arrows indicating the points of interest in the succeeding TEM micrographs. (c) A dark field (DF) TEM micrograph taken just before ITB migration shows an ITB/CTB junction forming a corner and step approximately 10 nm wide. (d) t ≈ 62.8 s: the ITB segment moved leftward, removing the remaining step that is 7.7 nm wide. The dotted red line indicates the initial ITB position. Arrows indicate the location of the large migration event, as well as two smaller events above. (e-h) Snapshots from simulated nanoindentation of nt Al and nt Cu with ITBs. Atoms are colored according to common-neighbor analysis. (e-f) Comparison of the initial and deformed microstructures of nt Al. Simulations show (1) ITB migration and vertical sliding via interface dislocations that nucleate from the surface, (2) lattice dislocations emitted from the region where indenter tip interacted with ITB, resulting in further ITB migration and sliding, and (3) migration and sliding are coupled together. (g-h) Comparison of the initial and final deformed nt Cu. MD simulations show that (i) ITB dissociates into 9R phase, (ii) dislocations emitted from indenter are blocked at ITB, and (iii) ITB migrates substantially and horizontally, but does not slide vertically. Dotted red lines indicate the initial ITB locations.

To investigate the details of ITB-dislocation interactions and ITB stability, we performed large-scale MD simulations on nanoindentation of nt Al (Fig. 11e-f). During indentation simulation, it is clear that 1) lattice dislocations nucleated at the contact surface and moved towards ITBs, and 2) ITBs blocked lattice dislocations, which then dissociated into interface disconnections. The interface disconnection has a Burgers vector of $\frac{1}{3}[111]$ and a step height of one $(11\bar{2})$ atomic plane. This process resulted in coupled shear-migration of ITBs in the vertical {111} direction, and the formation of horizontal steps at the ITB-dislocation interaction site.

For comparison, we also performed MD simulations for similarly structured low SFE nt Cu (Fig. 9g-h). Prior to absorption of the lattice dislocations, ITBs migrated and dissociated into two tilt walls bounding a volume of 9R phase due to applied shear stress. This dissociation process can accommodate plastic deformation in nt Cu. Thus, the ITB barrier resistance for lattice dislocations in nt Cu may not be as significant as those in nt Al.

In summary, *in situ* nanoindentation coupled with MD simulations revealed that ITBs in nt Al can effectively resist the pile-up of dislocations, and lead to significant work hardening. Repetitive dislocation-ITB interactions induced steps, where dislocation transmission eventually occurred, and ITB steps migrated to further accommodate plasticity at high stresses. This study provides a significant step forward towards quantitative understanding of ITB dominated plasticity in high strength nt Al, which could have wide spread applications.

I.7. The formation mechanisms of growth twins in polycrystalline Al

(Sichuang Xue, graduate students, Acta Mater, 2015)

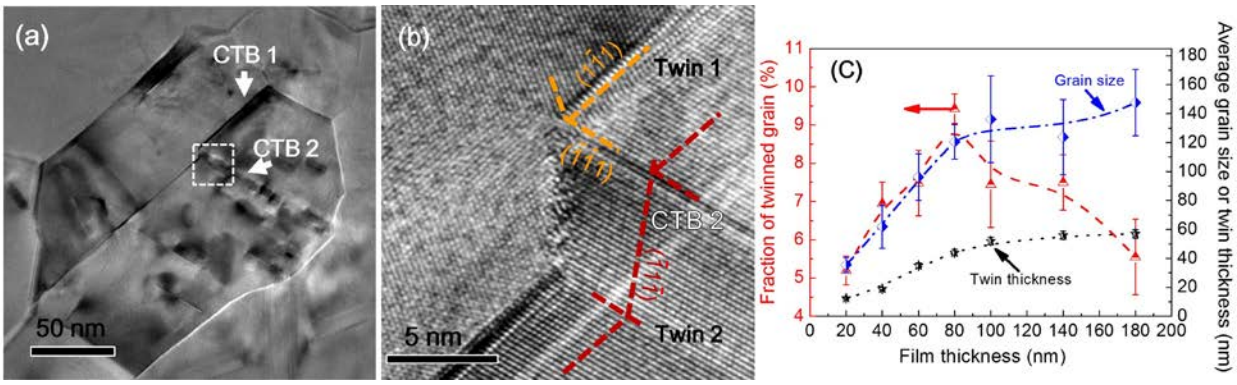

Figure 12. (a-b) Nanotwins formed in sputtered polycrystalline Al films. (c) The fraction of twinned grains reaches a maximum (9%) when film thickness is 80 nm.

Growth twins are scarcely observed in metals with high stacking fault energy, such as pure Al. In this study, however, we report the observation of growth twins in sputtered polycrystalline Al films on amorphous substrates and a majority of these growth twins are inclined to the growth direction (inclined twins, Fig. 12). Although the fraction of twinned grains is low, it increases monotonically with increasing film thickness, reaches a maximum (9%, Fig. 12c) at the film thickness of 80 nm, and decreases thereafter in the thicker films. The nucleation mechanism for the inclined twins is compared with that of the parallel growth twins in Al. Different twin formation

mechanisms are discussed. This study provides an alternative perspective to evaluate the formation of growth twins in metals with high stacking fault energy.

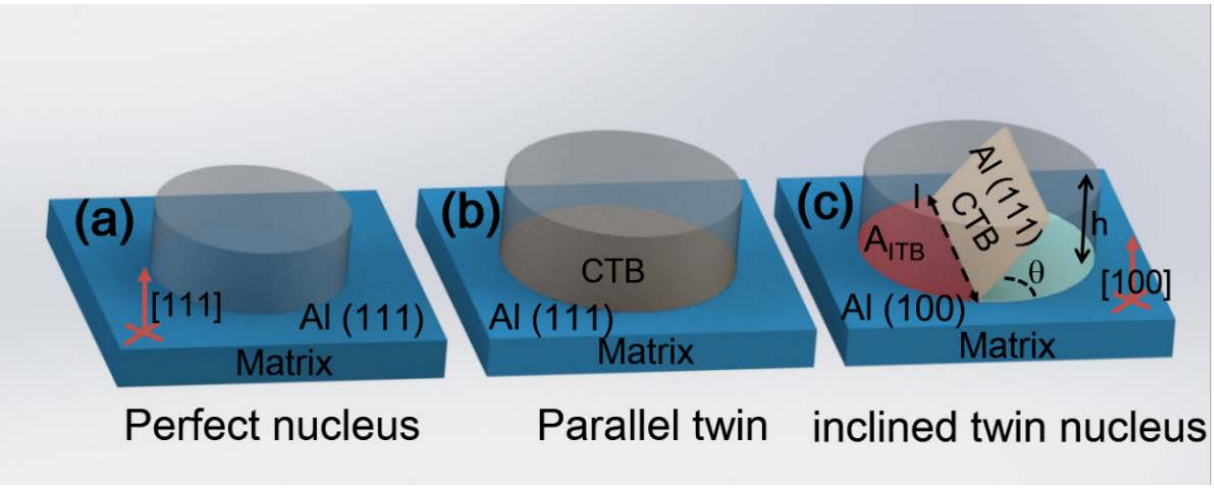

Figure 13. Schematic diagrams comparing the nucleation of (a) a perfect nucleus, (b) a parallel twinned nucleus and (c) a nucleus with inclined growth twin on Al matrix. (a) The perfect nucleus and the matrix has the same <111> crystal orientation. (b) The parallel twin nucleus forms (111) CTB on the (111) matrix. (c) A nucleus contains both inclined CTB and incoherent twin boundary (ITB) with the matrix. Note an example of (100) matrix is used to illustrate the concept without losing the generality of the model. A fraction of the matrix-nucleation interface contains ITB with an area of AITB, whereas the remaining of the nucleus has the same crystal orientation as that of the matrix.

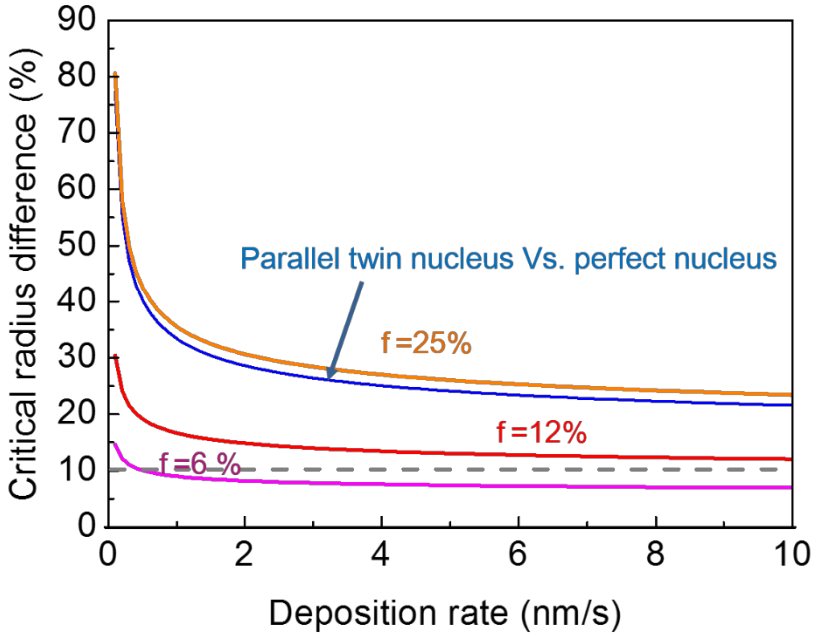

Figure 14. Plots of the percentage of critical radius difference between perfect nuclei and parallel twin nuclei Δrpara/rp (and between perfect and inclined twin nuclei Δrincl/rp, where Δrpara = rpara - rp, Δrincl = rincl - rp , and rp, rpara, rincl represent the radius of perfect, parallel and inclined twin nuclei respectively.

For parallel twins, rpara is at least 25% greater than that of rp even at a very high deposition rate, implying the nucleation of parallel growth twins in Al is very difficult in comparison for inclined twins, by reducing the area fraction of AITB to 12% (or less) of the contact area (between matrix and twin nuclei), rincl is merely ~ 10% greater than that of rp, implying the nucleation of inclined twins in Al is easier than the nucleation of parallel twins.

We compared the nucleation mechanisms of a perfect nucleus, a nucleus with a parallel twin and a nucleus with an inclined CTB as shown schematically in Fig. 13. The perfect nucleus in Fig. 13a has the {111} texture. The parallel twin nucleus in Fig. 13b has the same texture and the CTB is normal to the growth direction. For the inclined twin nucleus with {100} texture (the mechanism is similar for {110} texture), the {111} CTB formed a finite angle ($\neq 90^o$) with respect to the growth direction. As shown in Fig. 13c, the CTB separates the twin nucleus into a right and left section. The right portion of the nucleus has essentially a coherent interface with the matrix, whereas the left portion forms an ITB with the matrix. The angle θ between the CTB and the matrix/nucleus interface plane is the angle between (111) and (100) plane in this scenario. According to these different nucleation mechanisms, we calculated the critical radius difference between different nucleation models under different deposition rate (Figure 14). The result suggests that the probability for the formation of an inclined growth twin could be much greater than that of a parallel twin, consistent with the observation of predominantly inclined growth twins in polycrystalline Al with high SFE.

II. A list of papers published, in press, or accepted

1. Irene J. Beyerlein, Xinghang Zhang, and Amit Misra, Growth Twins and Deformation Twins in Metals, **Annu. Rev. Mater. Res.** 44 (2014) 15.1–15.35.
http://dx.doi.org/10.1146/annurev-matsci-070813-113304

Acknowledgement: X.Z. acknowledges financial support from DoE-OBES under grant number DE-SC0010482 for studies on mechanical behavior of NT Al.
(100% of support for Zhang)

2. KY Yu, D Bufford, Y Chen, Y Liu, H Wang, X Zhang, Basic criteria for formation of growth twins in high stacking fault energy metals, **Applied Physics Letters** 103 (2014) 181903.
http://dx.doi.org/10.1063/1.4826917

Acknowledgement: The work on twinning in Al was supported by DoE-OBES under Grant No. DE-SC0010482.
(50% support. There are student co-authors that are supported by other projects.)

3. Y. Liu, J. Hay, H. Wang, and X. Zhang, "A new method for reliable determination of strain-rate sensitivity of low-dimensional metallic materials by using nanoindentation", **Scripta Materialia,** 77 (2014) 5–8.

http://dx.doi.org/10.1016/j.scriptamat.2013.12.022

Acknowledgement: X.Z. acknowledges financial support by DoE OBES under Grant no. DE-SC0010482 for studies on mechanical behavior of nanotwinned metals.

4. Y. Liu, J. Jian, Y. Chen, H. Wang, and X. Zhang, Plasticity and ultra-low stress induced twin boundary migration in nanotwinned Cu by *in situ* nanoindentation studies, **Applied Physics Letters**, 104 (2014) 231910
http://dx.doi.org/10.1063/1.4882242

Acknowledgement: XZ acknowledges financial support by DoE-OBES under grant no. DE-SC0010482 for studies on mechanical behavior of nanotwinned metals.
(100% support)

5. D. Bufford, Y. Liu, J. Wang, H. Wang, X. Zhang. In situ nanoindentation study on sustainable plasticity and work hardening in nanotwinned aluminum, **Nature Communications**, 5 (2014).

http://dx.doi.org/10.1038/ncomms5864

Acknowledgement: XZ acknowledges financial support by DoE-OBES under grant no. DE-SC0010482.

(100% support for Zhang and his students)

6. Byung-Gil Yoo, Steven T. Boles, Y. Liu, X. Zhang, Ruth Schwaiger, Christoph Eberl, Oliver Kraft, Quantitative damage and detwinning analysis of nanotwinned copper foil under cyclic loading, ***Acta Materialia***, 81 (2014) 184-193.
http://dx.doi.org/10.1016/j.actamat.2014.08.021

Acknowledgement: XZ and YL acknowledge financial support by DoE-OBES under grant no. DE-SC0010482 for studies on mechanical behavior of nanotwinned metals. (100% of support for Zhang)

7. Y. Liu, N. Li, D. Bufford, J. Wang, J.H. Lee, H. Wang, and X. Zhang, *In situ* nanoindentation studies on detwinning and work hardening in nanotwinned monolithic metals”**,** ***JOM*** (invited review article), 68 (2016) 226.
http://dx.doi.org/10.1007/s11837-015-1518-1

Acknowledgement: XZ acknowledges financial support by DoE-OBES under grant no. DE-SC0010482

8. J. Li, K. Y. Yu, Y. Chen, M. Song, H. Wang, M.A. Kirk, M. Li, and X. Zhang, *In situ* Study of Defect Migration Kinetics and Self-Healing of Twin Boundaries in Heavy Ion Irradiated Nanotwinned Metals, ***Nano Letters***, 2015,

http://dx.doi.org/10.1021/nl504677z

Acknowledgement: KY Yu and the work on fabrication of nanotwinned metal are supported by DOE-OBES under grant no. DE-SC0010482.

9. S. Xue, Z. Fan, Y. Chen, J. Li, H. Wang, X. Zhang. The formation mechanisms of growth twins in polycrystalline Al with high stacking fault energy, **Acta Materialia**, 101 (2015) 62-70.

http://dx.doi.org/10.1016/j.actamat.2015.08.046

Acknowledgement: XZ acknowledges financial support by DoE-OBES under grant no. DE-SC0010482.

10. Y. Chen*, K.Y. Yu*, Y. Liu*, S. Shao, H. Wang, M.A. Kirk, J. Wang and X. Zhang, Damage tolerant nanotwinned metals with nanovoids under radiation environments, ***Nature Communications***, **6**, Article number 7036, doi:10.1038/ncomms8036, 2015.

http://dx.doi.org/10.1038/ncomms8036

Acknowledgement: Y.L. who works on fabrication of nanotwinned metals is supported by DOEOBES under grant no. DE-SC0010482.

11. Jin Li, Y. Chen, S. Xue, H. Wang, X. Zhang, Comparison of size dependent strengthening mechanisms in Ag/Fe and Ag/Ni multilayers, **Acta Materialia** 114 (2016) 154-163.
http://dx.doi.org/10.1016/j.actamat.2016.05.030

Acknowledgement: S. Xue is supported by DoE-OBES under grant No. DE-SC0010482.

12. Jian Wang and Xinghang Zhang, Twinning effects on strength and plasticity of metallic materials, **MRS Bulletin**, 47 (2016) 274.
https://doi.org/10.1557/mrs.2016.67

Acknowledgement: X.Z. acknowledges financial support by DoE-OBES under Grant No. DE-SC0010482.

13. Z. Fan, S. Xue, J. Wang, K.Y. Yu, H. Wang, X. Zhang, Unusual size dependent strengthening mechanisms of Cu/amorphous CuNb multilayers, **Acta Materialia** 120 (2016) 327-336.
http://dx.doi.org/10.1016/j.actamat.2016.08.064

Acknowledgement: S. Xue is supported by DoE-OBES under grant No. DE-SC0010482.

III. Patent

Provisional patent accepted

Xinghang Zhang, Daniel Bufford, Yue Liu and Haiyan Wang, METHOD FOR PRODUCTING HIGH STACKING FAULT ENERGY (SFE) METAL FILMS AND COATINGS WITH HIGH-

DENSITY NANOSCALE TWIN BOUNDARIES, US provision patent accepted, full patent filed in fall 2015.

80% support

IV. A list of participants working on the project

Name	Title	Percentage of support
Xinghang Zhang	PI	8%
Daniel Bufford	Postdoc, now at Sandia National Lab	100% (for 2 months)
Kaiyuan Yu	Postdoc; now a faculty in China Petroleum University	100% (for 1 year)
Yue Liu	Ph.D., Graduated 2014, Now a postdoc at Los Alamos National Lab	100%
Sichuang Xue	Graduate student	100%
Qiang Li	Graduate student	100%

V. Collaborators

1. Prof. Jian Wang, Dept. Mechanical Engineering, University of Nebraska, Lincoln

2. Prof. Dr. Christoph Eberl, Deputy Director Fraunhofer IWM,
Groupleader Meso and Micro Mechanics
Professor Micro and Materials Mechanics, University Freiburg

VI. Project impact

VI.1. What is the impact on the development of the principal discipline(s) of the project?

- Our studies show that nanotwins can be introduced into metals with high stacking fault energy. This is surprising as such an observation is in drastic contrast to the general anticipation.
- We show two strategies that can effectively introduce growth twins in high-stacking-energy metals: 1) Use Ag as a template to introduce high density growth twins in epitaxial Al; 2) Show that the film thickness is important in determination of volume fraction of growth twins

- We prove that high density twin boundaries can lead to significant work hardening capability in nanotwinned Al
- We have published two review articles, one in Annual Review of Materials Research; and one in MRS Bulletin

VI.2. What is the impact on other disciplines?

- Provide a strategy to design ductile nanotwinned light-weight Al alloys
- We establish a new protocol that can correctly measure the strain rate sensitivity of all metallic materials via nanoindentation
- The review articles have wide spread impact in other field, including nanomechanics; nanostructure metallic materials.

VI.3. What is the impact on the development of human resources?

The project has involved 2 Postdocs, 2 Ph.D. students and 2 undergraduate students at Texas A&M University. 2 graduate students have become postdoc at DOE national Lab (Sandia and Los Alamos); 1 postdoc become faculty at a University.

The results will be disseminated to the PI's graduate and undergraduate classes (with 100 students each semester).

VI.4. What is the impact on physical resources that form infrastructure?

The project has supported the use of sputter system equipment and ex situ nanoindentor in the PI's laboratory, and in situ nanoindentation facility on campus. It will also enrich several courses offered by the PI and other faculty. Graduate and undergraduate students working on this project have access to the PI's sputter system and nanoindentor for their courses.

VI.5. What is the impact on institutional resources that form infrastructure?

Enhance curriculum, graduate and undergraduate student teaching, gain advanced nanofabrication ability.

VI.6. What is the impact on information resources that form infrastructure?

Disseminate results through various TAMU research websites.

VI.7. What is the impact on technology transfer?

High strength, ductile Al alloys have significant implications for a variety of industries, including automobile, aerospace, and defense industry.

VI.8. What is the impact on society beyond science and technology?

The project will recruit talented young students, who may become the next generation researchers and educators. One of the students who worked partially on this project, Dr. Yue Liu, have become a postdoc at Los Alamos National Laboratory; and Dr. Dan Bufford has become a postdoc at Sandia National Lab.

VII. An update list of other support (current and pending, federal and non-federal. See attached form). For each, indicate the overlap, if any, and/or delineation compared to the DOE-supported project.

Current:

1. Title: Fundamental mechanisms of removal of stacking fault tetrahedral by mobile low energy boundaries
Sponsor: NSF-DMR 1304101
PI share: ~$400 K
Location: Purdue University
Period: 09/2013 – 08/2017
Person-Months per Year Committed to the Project: 0.5

There is no overlap with the DOE project.

2. Title: Collaborative Research: deformation mechanisms of fcc and hcp Cobalt with high-density stacking faults
Sponsor: NSF – DMR 1508366
PI amount: $248K
Location: Purdue University
Period: 06/2015 – 5/2018
Person-Months per Year Committed to the Project: 0.15 month

There is no overlap with the DOE project.

3. Title: High strength and high ductility martensitic steels
Sponsor: NSF – DMR
Lead PI: K. Ted Hartwig

Co-PI: Xinghang Zhang
Co-PI amount: $200K
Location: Purdue University
Period: 8/2016 – 7/2019
Person-Months per Year Committed to the Project: 0.25 month

There is no overlap with the DOE project.

Pending:
1. Title: Acquisition of a suite of 3D EDX tomography and in situ heating and straining TEM Holders to probe the response of Nanomaterials
Sponsor: ONR – DURIP equipment proposal
PI: Xinghang Zhang
Co-PI: Haiyan Wang
Amount: $276K
Location: Purdue University
Period: 08/2017 – 07/2019
Person-Months per Year Committed to the Project: 0 month

2. Title: **Additive manufacturing of radiation tolerant ferritic/martensitic steels**
Sponsor: DOE-NEUP
PI: Yung Shin,
Co-PI: Xinghang Zhang,
Amount: $640 K
Location: Purdue University
Period: 10/2017 – 09/2020

VIII. Cost status: Show approved budget by the budget period, actual costs incurred by the date of the report and projected unspent funds at the end of the current budget period. If any cost-sharing is required, breakout by DOE share, recipient share and total costs
DOE approved budget: $450K
Actual cost (as of Aug. 14, 2016): $450K